THERMAL SHOCK IN A TRANSVERSELY ISOTROPIC CYLINDER CONTAINING AN ANNULAR CRACK

Naotake Noda
Department of Mechanical Engineering, Faculty of Engineering, Shizuoka University,
Hamamatsu, Shizuoka 432, Japan

and

Fumihiro Ashida
Department of Mechanical Engineering, Tsuyama National College of Technology, Tsuyama,
Okayama 708, Japan

Abstract—The present paper is concerned with a thermal shock problem in a transversely isotropic cylinder containing an annular crack. In analysing this problem, we propose a simple solution technique for transient thermoelastic problems in transversely isotropic solids. This problem can be formulated in terms of a triple-series equation by means of the method of successive approximation as well as the Fourier integral and Bessel series. The triple-series equation is reduced to a simultaneous algebraic equation by the application of Fourier and Neumann series. The stress intensity factors at the inner and outer crack tips are derived from the axial displacement. Numerical calculations of the stress intensity factors which are carried out for graphites and ceramics are compared with one another. Finally, we propose simple formulations expressing the maximum stress intensity factors as a function of Biot's number and crack length.

1. INTRODUCTION

With the advance of material technology, various engineering materials exhibiting anisotropy have been put to practical use. Among these are heat resistant materials. Graphites and ceramics are very important materials for structures subject to severe thermal environments such as those in nuclear power plants and space. Some of those materials possess transverse isotropy which is a kind of anisotropy. If there are cracks in such materials, they may fracture due to the stress concentration at the crack tip. Therefore, evaluating the magnitude of stress concentrations in transversely isotropic materials is very important for determining the safety of a material.

Many papers are written on steady thermoelastic crack problems, while only a few papers have studied transient thermoelastic crack problems. Noda *et al.* have investigated transient thermoelastic crack problems in isotropic infinite solids (Noda and Matsunaga, 1986; Noda *et al.*, 1986, 1988) as well as in transversely isotropic infinite solids (Ashida and Noda, 1987; Noda and Ashida, 1987a, b, 1988). However these problems have received little practical applications. Nied (1983, 1987), Kokini (1986a, b) and Noda *et al.* (1989) have analysed thermal shock problems in edge cracked plates. Nied and Erdogan (1983), Oliveira and Wu (1987) and Noda *et al.* (1989, 1990) have researched thermoelastic crack problems in cylinders subjected to cooling or thermal shock. Since these papers are written on transient thermal stresses in isotropic plates and cylinders, we cannot find other papers on transient thermoelastic crack problems in transversely isotropic plates or cylinders.

This paper is concerned with a thermal shock problem in a transversely isotropic infinite circular cylinder with an annular crack. Temperature gradients are large in thermal shock problems, which cause large stress gradients. Since some materials are sensitive to stress gradients, thermal shock problems are important. In the problem of an annular crack, it is seen that the stress intensity factor at the inner crack tip is larger than that at the outer crack tip and increases with decreasing inner radius of the annular crack. Once the growth of an annular crack begins at the inner crack tip, that crack extends to the center of the cylinder. Therefore, we think that calculating the magnitude of stress intensity factor

at the inner crack tip is very important. Up to now, no elastic problem in a cylinder with an annular crack has been studied because it was difficult to derive the stress intensity factors at the crack tips.

In analysing this subject, we propose a new solution technique for transient thermo-elastic problems in transversely isotropic solids. This solution technique is formulated in terms of two thermoelastic displacement potential functions and two displacement potential functions which are governed by very simple equations.

In the analysis of the temperature field, it is assumed that the presence of a crack should have no effect on the temperature distribution, because there is no heat transfer in the axial direction in this problem. The method of successive approximation as well as the Bessel series and the Fourier integral are used to satisfy the mechanical boundary conditions. Therefore, this problem can be formulated in terms of a triple-series equation which is reduced to a simultaneous algebraic equation by means of the Fourier series and the Neumann series. The stress intensity factors cannot be derived directly from the axial stress, they must be derived from the axial displacement.

Numerical calculations of the stress intensity factors at both inner and outer crack tips are carried out for a transversely isotropic graphite, an isotropic graphite, a beryllium oxide and a zircon, and compared with one another. The stress intensity factors have maximum values with respect to a time variable. Finally, we propose the simple formulations expressing the maximum stress intensity factors as a function of Biot's number and crack length. Since fairly accurate stress intensity factors can be derived from these simple formulations, we think that these simple formulations provide useful engineering data.

2. SOLUTION TECHNIQUE IN TRANSVERSELY ISOTROPIC SOLIDS

The stress–strain relations for axisymmetric problems are expressed by

$$\left.\begin{aligned}
\sigma_{rr} &= c_{11}\varepsilon_{rr}+c_{12}\varepsilon_{\theta\theta}+c_{13}\varepsilon_{zz}-\beta_1(T-T_0)\\
\sigma_{\theta\theta} &= c_{12}\varepsilon_{rr}+c_{11}\varepsilon_{\theta\theta}+c_{13}\varepsilon_{zz}-\beta_1(T-T_0)\\
\sigma_{zz} &= c_{13}\varepsilon_{rr}+c_{13}\varepsilon_{\theta\theta}+c_{33}\varepsilon_{zz}-\beta_3(T-T_0)\\
\sigma_{rz} &= 2c_{44}\varepsilon_{rz}
\end{aligned}\right\}, \tag{1}$$

where c_{ij} and β_i are the material constants of a transversely isotropic solid (Nowinski, 1978), and $T-T_0$ is the temperature rise. The strain–displacement relations are defined by

$$\varepsilon_{rr} = u_{r,r}, \quad \varepsilon_{\theta\theta} = \frac{u_r}{r}, \quad \varepsilon_{zz} = u_{z,z}, \quad \varepsilon_{rz} = \frac{u_{r,z}+u_{z,r}}{2}, \tag{2}$$

where the comma denotes partial differentiation with respect to a variable. The equations of equilibrium for axisymmetric problems which are represented by the displacements are given by

$$\left.\begin{aligned}
c_{11}\left\{u_{r,rr}+\frac{1}{r}u_{r,r}-\frac{1}{r^2}u_r\right\}+c_{44}u_{r,zz}+(c_{13}+c_{44})u_{z,rz} &= \beta_1(T-T_0)_{,r}\\
c_{44}\left\{u_{z,rr}+\frac{1}{r}u_{z,r}\right\}+c_{33}u_{z,zz}+(c_{13}+c_{44})\left\{u_{r,rz}+\frac{1}{r}u_{r,z}\right\} &= \beta_3(T-T_0)_{,z}.
\end{aligned}\right\} \tag{3}$$

In order to solve eqns (3), we introduce the potential functions Ω and Θ which are related to the displacements as follows:

$$u_r = \Omega_{,r}, \quad u_z = (k\Omega + \Theta)_{,z}, \tag{4}$$

where k is an unknown coefficient. Substituting eqns (4) into eqns (3), we find

$$\Delta_1\Omega + \frac{kc_{13} + (1+k)c_{44}}{c_{11}}\Omega_{,zz} = \frac{\beta_1}{c_{11}}(T - T_0) - \frac{c_{13} + c_{44}}{c_{11}}\Theta_{,zz}, \tag{5}$$

$$\Delta_1\Omega + \frac{kc_{33}}{c_{13} + (1+k)c_{44}}\Omega_{,zz} = \frac{1}{c_{13} + (1+k)c_{44}}[\beta_3(T - T_0) - c_{44}\Delta_1\Theta - c_{33}\Theta_{,zz}], \tag{6}$$

where

$$\Delta_1 = \frac{\partial^2}{\partial r^2} + \frac{1}{r}\frac{\partial}{\partial r}.$$

It is assumed that the coefficient of $\Omega_{,zz}$ of eqn (5) is equal to that of eqn (6):

$$\frac{kc_{13} + (1+k)c_{44}}{c_{11}} = \frac{kc_{33}}{c_{13} + (1+k)c_{44}} \equiv \mu. \tag{7}$$

Eliminating k from eqn (7), the following equation can be derived:

$$c_{11}c_{44}\mu^2 + (c_{13}^2 + 2c_{13}c_{44} - c_{11}c_{33})\mu + c_{33}c_{44} = 0. \tag{8}$$

Let μ_1 and μ_2 denote the roots of eqn (8), so k_1 and k_2 corresponding to μ_1 and μ_2 are given by

$$k_i = \frac{c_{11}\mu_i - c_{44}}{c_{13} + c_{44}} \quad (i = 1, 2). \tag{9}$$

Substitution of eqn (5) into eqn (6) yields

$$\Delta_1\Theta + \mu_2\Theta_{,zz} = -\frac{k_1\mu_2\beta_1 - \beta_3}{c_{44}}(T - T_0) \quad (\text{for } \mu = \mu_1), \tag{10}$$

$$\Delta_1\Theta + \mu_1\Theta_{,zz} = -\frac{k_2\mu_1\beta_1 - \beta_3}{c_{44}}(T - T_0) \quad (\text{for } \mu = \mu_2). \tag{11}$$

Now, we introduce a new potential function Ψ as follows:

$$\Omega = \Psi + d\Theta, \tag{12}$$

where d is unknown. In the case of $\mu = \mu_1$, substituting eqns (12) and (10) into eqn (5) in order, we have

$$\Delta_1\Psi + \mu_1\Psi_{,zz} + (\mu_1 - \mu_2)\left\{d + \frac{1}{k_1 - k_2}\right\}\Theta_{,zz} = \left\{\frac{\beta_1}{c_{11}} + d\frac{k_1\mu_2\beta_1 - \beta_3}{c_{44}}\right\}(T - T_0). \tag{13}$$

In order to eliminate the term of $\Theta_{,zz}$ from eqn (13), putting d as follows:

$$d = -\frac{1}{k_1 - k_2} \tag{14}$$

we obtain

$$\Delta_1 \Psi + \mu_1 \Psi_{,zz} = -\frac{k_2 \mu_1 \bar{\beta}_1 - \bar{\beta}_3}{(k_1 - k_2)c_{44}}(T - T_0). \tag{15}$$

While we can obtain the following equation for $\mu = \mu_2$ in the same way as the case of $\mu = \mu_1$:

$$\Delta_1 \Psi + \mu_2 \Psi_{,zz} = \frac{k_1 \mu_2 \bar{\beta}_1 - \bar{\beta}_3}{(k_1 - k_2)c_{44}}(T - T_0), \tag{16}$$

where

$$d = \frac{1}{k_1 - k_2}. \tag{17}$$

Now, setting anew,

$$\Theta = \Phi/d \tag{18}$$

eqns (10) and (11) become

$$\Delta_1 \Phi + \mu_2 \Phi_{,zz} = \frac{k_1 \mu_2 \bar{\beta}_1 - \bar{\beta}_3}{(k_1 - k_2)c_{44}}(T - T_0) \quad (\text{for } \mu = \mu_1), \tag{19}$$

$$\Delta_1 \Phi + \mu_1 \Phi_{,zz} = -\frac{k_2 \mu_1 \bar{\beta}_1 - \bar{\beta}_3}{(k_1 - k_2)c_{44}}(T - T_0) \quad (\text{for } \mu = \mu_2). \tag{20}$$

It is clear that not only eqn (15) and eqn (20) but also eqn (16) and eqn (19) are the same. Therefore, the governing equations obtained in the case of $\mu = \mu_1$ are the same as those in the case of $\mu = \mu_2$.

For the case of $\mu = \mu_1$, rewriting as follows:

$$\Psi = \phi_1 + \psi_1, \quad \Phi = \phi_2 + \psi_2 \tag{21}$$

eqns (15) and (19) lead to the governing equations of potential functions:

$$\Delta_1 \phi_1 + \mu_1 \phi_{1,zz} = \xi_1 (T - T_0), \quad \Delta_1 \phi_2 + \mu_2 \phi_{2,zz} = \xi_2 (T - T_0), \tag{22}$$

$$\Delta_1 \psi_1 + \mu_1 \psi_{1,zz} = 0, \quad \Delta_1 \psi_2 + \mu_2 \psi_{2,zz} = 0, \tag{23}$$

where ϕ_1 and ϕ_2 are the particular solutions and

$$\xi_1 = -\frac{k_2 \mu_1 \bar{\beta}_1 - \bar{\beta}_3}{(k_1 - k_2)c_{44}}, \quad \xi_2 = \frac{k_1 \mu_2 \bar{\beta}_1 - \bar{\beta}_3}{(k_1 - k_2)c_{44}}. \tag{24}$$

Equations (4) become

$$u_r = (\phi_1 + \phi_2)_{,r} + (\psi_1 + \psi_2)_{,r}, \quad u_z = (k_1 \phi_1 + k_2 \phi_2)_{,z} + (k_1 \psi_1 + k_2 \psi_2)_{,z}. \tag{25}$$

It is clear that eqns (22) cannot be applied to the case of $k_1 = k_2$ (i.e. $k_1 = k_2 = 1$ and $\mu_1 = \mu_2 \equiv \mu_0$). In this case, the following relationship is derived among the transversely isotropic material constants:

$$c_{13} + 2c_{44} = \sqrt{c_{11}c_{33}}.$$

There may be transversely isotropic materials which exhibit such a characteristic. Therefore, we must consider other potential functions for the case of $k_1 = k_2$. Now, the following potential functions are introduced:

$$\Omega = \Psi + e\Theta + fz\Theta_{,z}, \tag{26}$$

where e and f are unknowns. Substituting eqns (26) and (10) into eqn (5) in order, the following equations are derived:

$$\Delta_1 \Psi + \mu_0 \Psi_{,zz} + \left\{ 2\mu_0 f + \frac{c_{13} + c_{44}}{c_{11}} \right\} \Phi_{,zz}$$

$$= \left\{ \frac{\beta_1}{c_{11}} + e \frac{\mu_0 \beta_1 - \beta_3}{c_{44}} \right\} (T - T_0) + f \frac{\mu_0 \beta_1 - \beta_3}{c_{44}} z(T - T_0)_{,z}. \tag{27}$$

In order to eliminate the terms of $\Phi_{,zz}$ and $T - T_0$ from eqn (27), putting e and f as follows:

$$e = -\frac{c_{44}\beta_1}{c_{11}(\mu_0\beta_1 - \beta_3)}, \quad f = -\frac{c_{13} + c_{44}}{2\mu_0 c_{11}} \tag{28}$$

we have

$$\Delta_1 \Psi + \mu_0 \Psi_{,zz} = -\frac{(c_{13} + c_{44})(\mu_0 \beta_1 - \beta_3)}{2\mu_0 c_{11}c_{44}} z(T - T_0)_{,z}. \tag{29}$$

Setting anew,

$$\Phi = \phi_1/e + \psi, \quad \Psi = \phi_2 \tag{30}$$

the governing equations of potential functions are obtained from eqns (10) and (29):

$$\Delta_1 \phi_1 + \mu_0 \phi_{1,zz} = \xi_1(T - T_0), \quad \Delta_1 \phi_2 + \mu_0 \phi_{2,zz} = \xi_2 z(T - T_0)_{,z}, \tag{31}$$

$$\Delta_1 \psi + \mu_0 \psi_{,zz} = 0, \tag{32}$$

where ϕ_1 and ϕ_2 are the particular solutions and

$$\xi_1 = \frac{\beta_1}{c_{11}}, \quad \xi_2 = -\frac{(c_{13} + c_{44})(\mu_0 \beta_1 - \beta_3)}{2\mu_0 c_{11}c_{44}}. \tag{33}$$

Equations (4) become

$$u_r = \{ \phi_1 + j_2 z\phi_{1,z} + \phi_2 \}_{,r} + \psi_{,r}, \quad u_z = \{ j_1\phi_1 + j_2 z\phi_{1,z} + \phi_2 \}_{,z} + \psi_{,z}, \tag{34}$$

where

$$j_1 = -\frac{(c_{13} + c_{44})\beta_1 - c_{11}\beta_3}{c_{44}\beta_1}, \quad j_2 = -\frac{(c_{13} + c_{44})(\mu_0 \beta_1 - \beta_3)}{2\mu_0 c_{44}\beta_1}. \tag{35}$$

In the case of isotropic conditions, the coefficients become

$$\mu_0 = 1, \quad \xi_1 = \frac{1+\nu}{1-\nu}\alpha, \quad \xi_2 = 0, \quad j_1 = 1, \quad j_2 = 0,$$

where ν is Poisson's ratio and α is the coefficient of linear thermal expansion. Omitting one for ϕ_2, since the governing equations of ϕ_2 and ψ are the same, the potential functions ϕ_1 and ψ correspond to Goodier's thermoelastic potential function and the first of Boussinesq's functions.

3. THERMAL SHOCK IN A TRANSVERSELY ISOTROPIC CYLINDER WITH AN ANNULAR CRACK

3.1. *Temperature field*

Let us consider a heat conduction problem for a transversely isotropic infinite circular cylinder containing an annular crack, as shown in Fig. 1. The infinite cylinder, initially at the same uniform temperature T_0, is suddenly subjected to the higher temperature T_b on the outer radius of the cylinder. The temperature T_b is constant in the circumferential and axial directions. Since there is no heat transfer in the axial direction in this problem, it may be assumed that the presence of a crack should have no effect on the temperature distribution in this idealized case. Therefore, the temperature distribution varies in the radial direction, but does not vary in the axial direction.

The governing equation for transient heat conduction is given by

$$T_{,rr} + \frac{1}{r} T_{,r} = \frac{T_{,t}}{\kappa_r}, \tag{36}$$

where t is the time variable and κ_r is the thermal diffusivity.

The initial and boundary conditions for temperature field are expressed by

$$T = T_0 \quad \text{at } t = 0, \tag{37}$$

$$T_{,r} = -\frac{h}{\lambda_r}(T - T_b) \quad \text{on } r = a, \tag{38}$$

where h is the coefficient of heat transfer on the outer radius of the cylinder and λ_r is the coefficient of thermal conductivity in the radial direction.
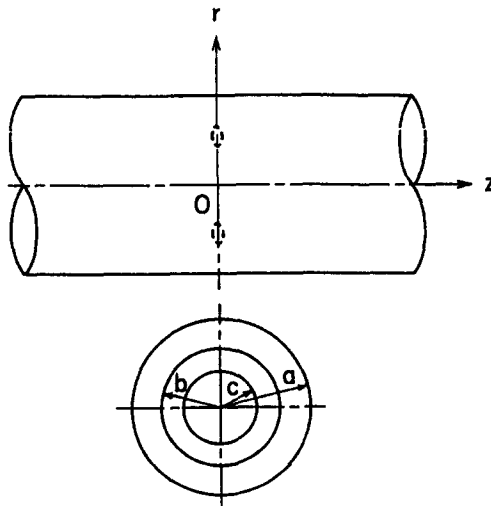

Fig. 1. Transversely isotropic cylinder with annular crack.

In this heat conduction problem, the temperature distribution is given by Carslaw and Jaeger (1967) as follows:

$$T = T_0 + (T_b - T_0) \left\{ 1 - \sum_{m=1}^{\infty} T_m J_0(\beta_m r) \right\}, \tag{39}$$

where

$$T_m = \frac{2h \cdot \exp(-\kappa_r \beta_m^2 t)}{a \lambda_r (\beta_m^2 + h^2/\lambda_r^2) J_0(\beta_m a)} \tag{40}$$

and β_m are the roots of the equation:

$$\beta J_1(\beta a) - \frac{h}{\lambda_r} J_0(\beta a) = 0 \tag{41}$$

and where $J_n(r)$ is the Bessel function.

3.2. Thermal stresses

Let us consider a transient thermoelastic problem in a transversely isotropic infinite circular cylinder containing an annular crack.

We assume the following admissible solutions for the potential functions ϕ_1, ϕ_2, ψ_1 and ψ_2 governed by eqns (22) and (23):

$$\phi_i = \xi_i (T_b - T_0) \left\{ \frac{r^2}{4} + \sum_{m=1}^{\infty} \beta_m^{-2} T_m J_0(\beta_m r) \right\} \quad (i = 1, 2), \tag{42}$$

$$\psi_i = -(T_b - T_0) \left[D_i \left(\frac{r^2}{4} - \frac{z^2}{2\mu_i} \right) + \sum_{m=1}^{\infty} \beta_m^{-2} E_{im} J_0(\beta_m r) \exp\left(-\frac{\beta_m z}{\sqrt{\mu_i}} \right) \right. $$
$$\left. + \int_0^{\infty} p^{-2} F_{ip} I_0(p\sqrt{\mu_i} r) \cos(pz)\, dp \right] \quad (i = 1, 2), \tag{43}$$

where ξ_1 and ξ_2 are given by eqns (24), D_i, E_{im} and F_{ip} are unknown coefficients, and $I_n(r)$ is the modified Bessel function.

The substitution of eqns (39), (42) and (43) into eqns (25), (2) and (1) leads to these displacements and stresses:

$$u_z = (T_b - T_0) \sum_{i=1}^{2} \left[\frac{k_i}{\mu_i} D_i z + \sum_{m=1}^{\infty} \frac{k_i}{\beta_m \sqrt{\mu_i}} E_{im} J_0(\beta_m r) \exp\left(-\frac{\beta_m z}{\sqrt{\mu_i}} \right) \right. $$
$$\left. + \int_0^{\infty} p^{-1} k_i F_{ip} I_0(p\sqrt{\mu_i}\, r) \sin(pz)\, dp \right], \tag{44}$$

$$\sigma_{zz} = -(T_b - T_0) \left[\sum_{i=1}^{2} (c_{13}\mu_i - c_{33}k_i) \left[\frac{D_i}{\mu_i} - \sum_{m=1}^{\infty} \frac{E_{im}}{\mu_i} J_0(\beta_m r) \exp\left(-\frac{\beta_m z}{\sqrt{\mu_i}} \right) \right. \right. $$
$$\left. \left. + \int_0^{\infty} F_{ip} I_0(p\sqrt{\mu_i}\, r) \cos(pz)\, dp \right] - (c_{13}\xi_1 - \beta_3) \left\{ 1 - \sum_{m=1}^{\infty} T_m J_0(\beta_m r) \right\} \right], \tag{45}$$

where the other displacement and stresses are omitted here.

The boundary conditions for the displacement and stresses are given by:

$$\int_0^a \sigma_{zz} r \, \mathrm{d}r = 0 \quad \text{at } z \to \infty, \tag{46}$$

$$\sigma_{rr} = \sigma_{zr} = 0 \quad \text{on } r = a, \tag{47}$$

$$\sigma_{rz} = 0 \quad \text{on } z = 0, \tag{48}$$

$$u_z = 0 \quad (0 \leqslant r \leqslant c, b \leqslant r \leqslant a), \quad \sigma_{zz} = 0 \, (c < r < b) \quad \text{on } z = 0. \tag{49}$$

The coefficients can be determined by eqns (46)–(49). In order to solve eqns (47)–(49), we apply the Fourier integrals of sin (pz) and cos (pz) and the Bessel series of $J_0(\beta_m r)$. F_1 and F_2 can be determined from eqn (46) and the constant term of the first of eqns (47). The other coefficients are determined by means of the method of successive approximation. The $(2j)$th approximation is a solution that satisfies eqns (47) and the $(2j+1)$th approximation is a solution that satisfies eqns (48) and (49). We obtain the following equations from the terms of $J_0(\beta_m r)$ of eqns (47):

$$E_{ip}^{2j} = \sum_{m=1}^{\infty} \{\Psi_{i1} D_{1m}^{2j+1} + \Psi_{i2} D_{2m}^{2j+1}\} \quad (i = 1, 2) \ (j = 0, 1, 2, \ldots). \tag{50}$$

Equation (48) gives

$$D_{2m}^{2j+1} = \Psi_3 D_{1m}^{2j+1} \quad (j = 0, 1, 2, \ldots). \tag{51}$$

Here Ψ_{i1}, Ψ_{i2} and Ψ_3 are known coefficients but are omitted. Equations (49) reduce to the following triple-series equation:

$$\left.\begin{aligned}
[u_z]_{z=0} &= (T_b - T_0) \sum_{m=1}^{\infty} \Phi_1 \, D_{1m}^{2j+1} J_0(\beta_m r) \\
&= 0 \quad (0 \leqslant r \leqslant c, \, b \leqslant r \leqslant a), \\
[\sigma_{zz}]_{z=0} &= (T_b - T_0) \sum_{m=1}^{\infty} [\Phi_2 D_{1m}^{2j+1} + \delta_{j0}\Omega_{1m} + (1-\delta_{j0})\Omega_{2m}^{2j}] J_0(\beta_m r) \\
&= 0 \quad (c < r < b),
\end{aligned}\right\} \quad (j = 0, 1, 2, \ldots), \tag{52}$$

where

$$\Omega_{1m} = \Gamma_0 T_m + \Gamma_1 F_1 + \Gamma_2 F_2 + \Gamma_3, \quad \Omega_{2m}^{2j} = \int_0^{\infty} \{\Gamma_4 E_{1p}^{2j} + \Gamma_5 E_{2p}^{2j}\} \, \mathrm{d}p \tag{53}$$

and where Φ_i and Γ_i are known coefficients but are omitted here, and δ_{j0} is Kronecker's delta. In order to solve the triple-series equation, we introduce the following function which identically satisfies the first of eqns (52):

$$\sum_{m=1}^{\infty} \Phi_1 \, D_{1m}^{2j+1} J_0(\beta_m r) = \frac{1}{r_c r_w} \sum_{n=1}^{\infty} x_n^{2j+1} \sin(n\theta), \tag{54}$$

where x_n^{2j+1} are unknowns, and

$$r^2 = r_c^2 + r_w^2 - 2r_c r_w \cos\theta, \quad r_c = \frac{b+c}{2}, \quad r_w = \frac{b-c}{2}. \tag{55}$$

Applying the inverse Hankel transform to eqn (54), D_{1m} are expressed by

$$D_{1m}^{2j+1} = \frac{1}{\Phi_1} \sum_{n=1}^{\infty} L_{mn} x_n^{2j+1} \quad (m = 1, 2, 3, \ldots), \tag{56}$$

where

$$L_{mn} = \frac{\pi \beta_m^2}{a^2 (\beta_m^2 + h^2/\lambda_r^2) J_0^2(\beta_m a)} Z_{nm} \tag{57}$$

and where

$$Z_{nm} = J_{n-1}(\beta_m r_c) J_{n-1}(\beta_m r_w) - J_{n+1}(\beta_m r_c) J_{n+1}(\beta_m r_w). \tag{58}$$

Substituting eqns (56) into the second of eqns (52) and applying the Neumann series,

$$J_0\left(\sqrt{\zeta_1^2 + \zeta_2^2 - 2\zeta_1 \zeta_2 \cos\theta}\right) = J_0(\zeta_1) J_0(\zeta_2) + 2 \sum_{k=1}^{\infty} J_k(\zeta_1) J_k(\zeta_2) \cos(k\theta) \tag{59}$$

we get the following infinite system of simultaneous algebraic equations which determines the unknowns:

$$\sum_{n=1}^{\infty} x_n^{2j+1} \sum_{m=1}^{\infty} \frac{\Phi_2}{\Phi_1} L_{mn} Z_{km} = - \sum_{m=1}^{\infty} [\delta_{j0} \Omega_{1m} + (1 - \delta_{j0}) \Omega_{2m}^{2j}] Z_{km}, \quad (k = 1, 2, 3, \ldots). \tag{60}$$

3.3. Stress intensity factors

We will define the stress intensity factors from the axial displacement. The stress intensity factor at the inner crack tip K_{Ii} and that at the outer crack tip K_{Io} are given by

$$K_{Ii} = -\sqrt{\frac{\pi}{2}} \cdot \Lambda \cdot \lim_{r \to c^+} \frac{[u_z]_{z=0}}{\sqrt{r-c}}, \quad K_{Io} = -\sqrt{\frac{\pi}{2}} \cdot \Lambda \cdot \lim_{r \to b^-} \frac{[u_z]_{z=0}}{\sqrt{b-r}}, \tag{61}$$

where

$$\Lambda = \frac{\sqrt{\mu_1}(1+k_2)(c_{13} - c_{33} k_1/\mu_1) - \sqrt{\mu_2}(1+k_1)(c_{13} - c_{33} k_2/\mu_2)}{k_1 - k_2}. \tag{62}$$

The axial displacement on $z = 0$ is obtained from the first of eqns (52) and eqn (54) as follows:

$$[u_z]_{z=0} = \frac{T_b - T_0}{r_c r_w} \sum_{n=1}^{\infty} \sum_{j=0}^{\infty} x_n^{2j+1} \sin(n\theta). \tag{63}$$

Substituting eqn (63) into eqns (61), the stress intensity factors are expressed by

$$\left. \begin{aligned} K_{Ii} &= -(T_b - T_0) \frac{\sqrt{\pi c} \cdot \Lambda}{(r_c r_w)^{3/2}} \sum_{n=1}^{\infty} n \sum_{j=0}^{\infty} x_n^{2j+1} \\ K_{Io} &= -(T_b - T_0) \frac{\sqrt{\pi b} \cdot \Lambda}{(r_c r_w)^{3/2}} \sum_{n=1}^{\infty} (-1)^{n-1} n \sum_{j=0}^{\infty} x_n^{2j+1} \end{aligned} \right\}. \tag{64}$$

3.4. Numerical examples

For convenience in numerical calculations, the following dimensionless quantities are

Table 1. Material constants of transversely isotropic graphite, isotropic graphite, beryllium oxide and zircon (c_{ij}: $\times 10^9$ Pa, α_i: $\times 10^{-6}$ K^{-1})

Materials	c_{11}	c_{12}	c_{13}	c_{33}	c_{44}	α_r	α_z
TG	10.71	1.34	1.50	12.18	4.14	3.9	3.5
IG	10.71	1.34	1.34	10.71	4.68	3.9	3.9
BO	470	168	119	494	153	2.3	4.4
ZC	258.5	179.1	154.2	380.5	73.3	6.6	7.7

introduced :

$$t' = \frac{\kappa_r t}{a^2}, \quad B_i = \frac{ah}{\lambda_r}, \quad \gamma = \frac{b-c}{a}, \quad \eta = \frac{b}{a} \quad (\hat{K}_{Ii}, \hat{K}_{Io}) = \frac{(K_{Ii}, K_{Io})}{\sqrt{b-c} \, \alpha_r E_r (T_b - T_0)}, \quad (65)$$

where E_r, E_z and G_{rz} are the moduli of elasticity, α_r and α_z are the coefficients of linear thermal expansion, t' is Fourier's number, and B_i is Biot's number.

The numerical calculations are carried out for a transversely isotropic graphite (TG), an isotropic graphite (IG), a beryllium oxide (BO) and a zircon (ZC). Those material constants are shown in Table 1.

It is necessary to examine the convergences of infinite series involving eqns (60) and (64). The upper limits of infinite series of $\sum_{m=1}^{\infty}$, $\sum_{m'=1}^{\infty}$, $\sum_{n=1}^{\infty}$ and $\sum_{j=0}^{\infty}$ are represented by M, M', N and J, where $\sum_{m=1}^{\infty}$ and $\sum_{m'=1}^{\infty}$ denote the infinite series of the left- and right-hand sides of eqns (60), respectively. The stress intensity factors at the inner and outer crack tips of the TG cylinder are calculated for various upper limit numbers of these infinite series. The calculated results are shown in Table 2. It is clear from this table that infinite series converge for $M = 8000$, $M' = 60$, $N = 5$ and $J = 4$ at a reasonable rate.

Figures 2 and 3 illustrate the time variations of stress intensity factors at the inner and outer crack tips for various Biot numbers. The solid and broken lines represent the stress intensity factors calculated for TG and IG. Both stress intensity factors for TG are somewhat larger than those for IG. The stress intensity factor at the inner crack tip is larger than that at the outer crack tip. It is seen from these figures that both stress intensity factors have maximum values with respect to Fourier's number and increase according to Biot's number. The maximum stress intensity factor at the inner crack tip appears later than that at the outer crack tip, because the distance from the outer surface of the cylinder to the inner crack tip is longer than that to the outer crack tip. Figures 4 and 5 show the effect of crack length on the maximum stress intensity factors at the inner and outer crack tips, in which the maximum stress intensity factor at the outer crack tip for $\gamma = 0.7$ is calculated from the case of a penny-shaped crack. Both maximum stress intensity factors increase according to crack length, and the maximum stress intensity factor at the outer crack tip gets close to that of penny-shaped crack. Therefore, once the growth of an annular crack begins at the inner crack tip, that crack extends to the center of the cylinder. Figures 6 and 7 illustrate

Table 2. Effects of upper limit numbers of infinite series on stress intensity factors at inner and outer crack tips for transversely isotropic graphite ($\eta = 0.7$, $\gamma = 0.5$, $B_i = 1$) (K_{Ii}, K_{Io}: $\times 10^{-2}$)

|				Fourier's number t'							
Upper limits of series				10^{-3}		10^{-2}		10^{-1}		10^0	
M	M'	N	J	$\hat{K}_{Ii}$	$\hat{K}_{Io}$	$\hat{K}_{Ii}$	$\hat{K}_{Io}$	$\hat{K}_{Ii}$	$\hat{K}_{Io}$	$\hat{K}_{Ii}$	$\hat{K}_{Io}$
8000	60	5	4	0.310	0.282	2.905	2.547	9.655	4.124	2.617	0.872
6000	60	5	4	0.310	0.283	2.907	2.550	9.660	4.129	2.618	0.874
10000	60	5	4	0.310	0.282	2.904	2.546	9.652	4.122	2.616	0.872
8000	50	5	4	0.308	0.288	2.904	2.552	9.654	4.129	2.616	0.874
8000	70	5	4	0.309	0.285	2.905	2.549	9.655	4.126	2.616	0.873
8000	60	4	4	0.309	0.283	2.901	2.543	9.639	4.109	2.612	0.868
8000	60	6	4	0.310	0.282	2.905	2.547	9.659	4.120	2.617	0.872
8000	60	5	2	0.310	0.283	2.903	2.545	9.650	4.120	2.615	0.872
8000	60	5	6	0.310	0.282	2.905	2.547	9.655	4.124	2.617	0.872
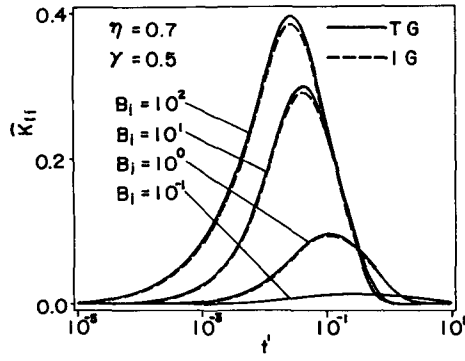
Fig. 2. Time variations of stress intensity factors at inner crack tip for transversely isotropic graphite and isotropic graphite.
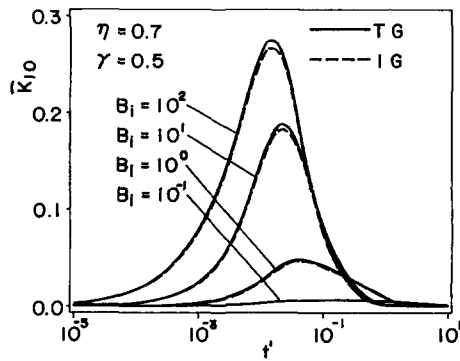

Fig. 3. Time variations of stress intensity factors at outer crack tip for transversely isotropic graphite and isotropic graphite.
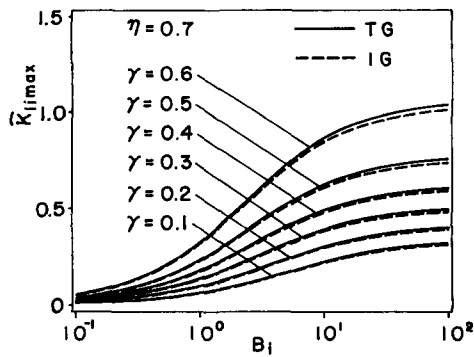

Fig. 4. Relations between maximum stress intensity factor at inner crack tip and Biot's number for transversely isotropic graphite and isotropic graphite.
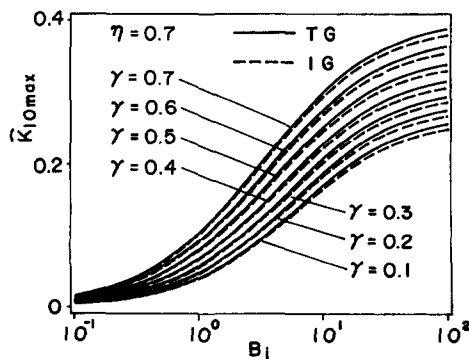

Fig. 5. Relations between maximum stress intensity factor at outer crack tip and Biot's number for transversely isotropic graphite and isotropic graphite.
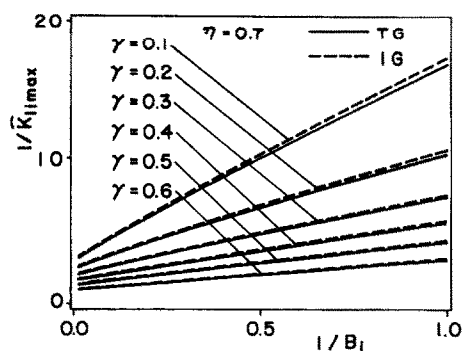
Fig. 6. Relations between reciprocal of maximum stress intensity factor at inner crack tip and that of Biot's number for transversely isotropic graphite and isotropic graphite.
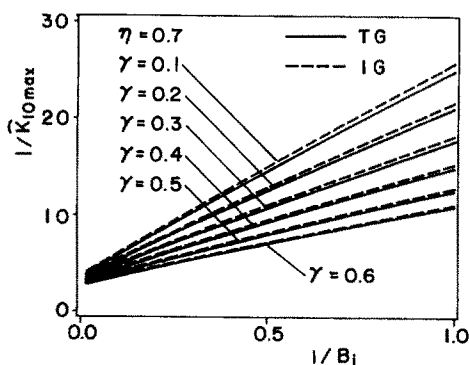

Fig. 7. Relations between reciprocal of maximum stress intensity factor at outer crack tip and that of Biot's number for transversely isotropic graphite and isotropic graphite.

how the reciprocals of maximum stress intensity factors at the inner and outer crack tips depend on the reciprocal of Biot's number. Next, Figs 8 and 9 illustrate the effects of anisotropic parameters on the reciprocals of the maximum stress intensity factors at the inner and outer crack tips. These figures show that both maximum stress intensity factors are greatly dependent on the anisotropic parameters.

From Figs 6–9, both reciprocals of the maximum stress intensity factors for small Biot numbers can be expressed by linear functions of the reciprocal of Biot's number, but those for larger Biot numbers deviate from the linear functions. Therefore, we propose the
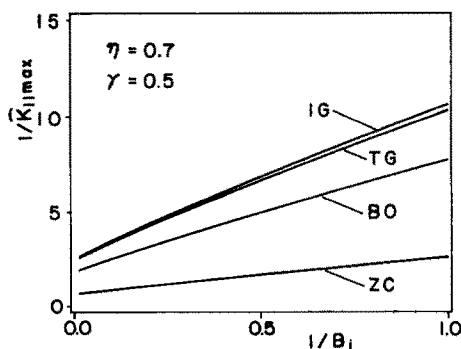

Fig. 8. Differences among maximum stress intensity factors at inner crack tip for transversely isotropic graphite, isotropic graphite, beryllium oxide and zircon.
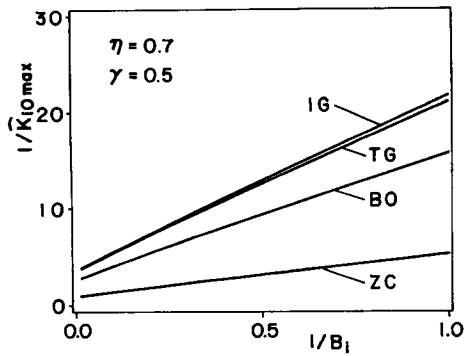
Fig. 9. Differences among maximum stress intensity factors at outer crack tip for transversely isotropic graphite, isotropic graphite, beryllium oxide and zircon.

following equations:

$$\left.\begin{array}{l}\dfrac{1}{\hat{K}_{Ii\,max}} = \dfrac{d_1}{B_i} + \dfrac{d_2}{\sqrt{B_i}} + d_3 \\[4mm] \dfrac{1}{\hat{K}_{Io\,max}} = \dfrac{e_1}{B_i} + \dfrac{e_2}{\sqrt{B_i}} + e_3\end{array}\right\} \quad (0.1 \leqslant B_i \leqslant 100, \quad \eta = 0.7). \tag{66}$$

The coefficients are determined by the method of least squares, and using the technique once more, the coefficients can be expressed as a function of crack length as follows:

$$\left.\begin{array}{l}\ln(d_1) = 3.638\gamma^2 - 6.095\gamma + f_{10} \\[2mm] \ln(d_2) = -5.013\gamma^2 - 0.355\gamma + f_{20} \\[2mm] \ln(d_3) = -0.743\gamma^2 - 1.650\gamma + f_{30} \\[2mm] \ln(e_1) = 0.857\gamma^2 - 2.929\gamma + g_{10} \\[2mm] \ln(e_2) = -9.763\gamma^2 + 8.520\gamma + g_{20} \\[2mm] \ln(e_3) = 0.701\gamma^2 - 1.277\gamma + g_{30}\end{array}\right\} \quad (0.1 \leqslant \gamma \leqslant 0.6, \quad \eta = 0.7), \tag{67}$$

where f_{i0} and g_{i0} are given in Table 3. The calculated values of the coefficients of γ^2 and γ for the four materials are almost the same, so we use the average values of those. As the accuracy of eqns (66) is important, we examine the relative errors between the maximum stress intensity factors at the inner and outer crack tips calculated from eqns (64) and those calculated from eqns (66). The results for TG and IG are shown in Tables 4 and 5. The

Table 3. Calculated values of f_{i0} and g_{i0} ($\eta = 0.7$)

Materials	f_{10}	f_{20}	f_{30}	g_{10}	g_{20}	g_{30}
TG	3.017	0.639	1.186	3.326	−1.036	1.418
IG	3.047	0.678	1.216	3.358	−0.966	1.446
BO	2.724	0.346	0.894	3.033	−1.326	1.125
ZC	1.616	−0.762	−0.215	1.924	−2.433	0.016

Table 4. Relative errors of maximum stress intensity factors at inner and outer
crack tips for transversely isotropic graphite ($\eta = 0.7$)

	$\hat{K}_{Ii\,max}$ (%)				$\hat{K}_{Io\,max}$ (%)			
	B_i				B_i			
γ	0.1	1	10	100	0.1	1	10	100
0.1	4.9	3.4	1.0	4.1	−1.9	−1.4	−1.8	−0.8
0.2	−6.3	−3.5	−3.3	0.9	2.5	2.0	0.4	1.9
0.3	−3.0	−2.6	−3.4	1.0	2.0	1.7	−0.1	2.8
0.4	3.5	2.2	−0.2	3.4	−1.6	−0.2	−1.5	2.9
0.5	6.0	5.3	1.8	5.5	−2.2	−1.6	−2.4	2.5
0.6	−4.2	−2.7	−3.9	−0.6	1.6	1.4	−0.8	2.3

Table 5. Relative errors of maximum stress intensity factors at inner and outer
crack tips for isotropic graphite ($\eta = 0.7$)

	$\hat{K}_{Ii\,max}$ (%)				$\hat{K}_{Io\,max}$ (%)			
	B_i				B_i			
γ	0.1	1	10	100	0.1	1	10	100
0.1	4.9	3.4	1.0	4.1	−1.9	−1.4	−1.8	−0.7
0.2	−6.3	−3.5	−3.3	0.9	2.5	1.9	0.3	1.9
0.3	−3.0	−2.6	−3.4	1.0	2.0	1.7	−0.1	2.8
0.4	3.5	2.2	−0.2	3.4	−1.6	−0.2	−1.4	2.9
0.5	6.0	5.3	1.8	5.5	−2.2	−1.6	−2.4	2.5
0.6	−4.2	−2.7	−3.9	−0.6	1.6	1.4	−0.8	2.3

maximum relative errors of the maximum stress intensity factors at the inner and outer crack tips for TG are 6.4% and 2.7%, respectively, and those for IG are 6.4% and 3.7%. Those for BO are 6.3% and 3.1% and for ZC are 6.5% and 3.3%, respectively. Fairly accurate values of the maximum stress intensity factors for each material can be simply calculated from eqns (66). Thus, these approximate equations can give useful engineering data.

REFERENCES

Ashida, F. and Noda, N. (1987). Study of transient thermal stress for a penny-shaped crack in a transversely isotropic infinite solid. *Theoret. Appl. Mech.* **35**, 305–311.
Carslaw, H. S. and Jaeger, J. C. (1967). *Conduction of Heat in Solids.* Oxford University Press, Oxford.
Kokini, K. (1986a). On the use of the finite element method for the solution of a cracked strip under thermal shock. *Engng Fract. Mech.* **24**, 843–850.
Kokini, K. (1986b). Thermal shock of a cracked strip : effect of temperature-dependent material properties. *Engng Fract. Mech.* **25**, 167–176.
Nied, H. F. (1983). Thermal shock fracture in an edge-cracked plate. *J. Thermal Stresses* **6**, 217–229.
Nied, H. F. (1987). Thermal shock in an edge-cracked plate subjected to uniform surface heating. *Engng Fract. Mech.* **26**, 239–246.
Nied, H. F. and Erdogan, F. (1983). Transient thermal stress problem for a circumferentially cracked hollow cylinder. *J. Thermal Stresses* **6**, 1–14.
Noda, N. and Ashida, F. (1987a). Stress intensity factor for transient thermal stresses on a transversely isotropic infinite body with an external circular crack. *Acta Mech.* **66**, 217–231.
Noda, N. and Ashida, F. (1987b). Transient thermoelastic fields in a transversely isotropic infinite solid with a penny-shaped crack. *J. Appl. Mech.* **54**, 854–860.
Noda, N. and Ashida, F. (1988). Stress intensity factors for a transversely isotropic infinite solid containing an annular crack. *J. Thermal Stresses* **11**, 39–55.
Noda, N. and Matsunaga, Y. (1986). Transient thermoelastic problem in an infinite body containing a penny-shaped crack due to time and position dependent temperature condition. *ZAMM* **66**, 233–239.
Noda, N., Matsunaga, Y. and Nyuko, H. (1986). Stress intensity factor for transient thermal stresses in an infinite elastic body with an external crack. *J. Thermal Stresses* **9**, 119–131.
Noda, N., Matsunaga, Y. and Nyuko, H. (1988). Stress intensity factor for transient thermal stresses in an infinite elastic solid containing an annular crack. *Ing.-Arch.* **58**, 1–8.
Noda, N., Matsunaga, Y. and Nyuko, H. (1990). Thermal shock problem of a hollow circular cylinder with a crack. *Int. J. Press. Vess. Piping* **42**, 247–257.
Noda, N., Matsunaga, Y., Tsuji, T. and Nyuko, H. (1989). Thermal shock problems of elastic bodies with a crack. *J. Thermal Stresses* **12**, 369–383.
Nowinski, J. L. (1978). *Theory of Thermoelasticity with Applications.* Sijthoff & Noordhoff, The Netherlands.
Oliveira, R. and Wu, X. R. (1987). Stress intensity factors for axial cracks in hollow cylinders subjected to thermal shock. *Engng Fract. Mech.* **27**, 185–197.